A Self-Occluding He-3 Neutron Detector for Reliable Surveillance of Spent Fuel Cask Movement

Marc L. Ruch, Lee A. ReFalo, and Thierry P. Pochet

International Atomic Energy Agency, Vienna, Austria

Abstract

The International Atomic Energy Agency (IAEA) uses Unattended Monitoring Systems (UMS) to support safeguarding nuclear material in facilities around the world. These UMS are required to operate continuously without the intervention of inspectors or technicians. Some UMS are used for monitoring the movements of dry casks containing spent fuel. This can be done by placing multiple neutron detectors throughout a facility and observing the relative change in neutron count rates as the cask is moved. However, options for the positioning of these detectors are often limited and emplacing multiple detectors can be costly. Being able to reliably track the movement of a spent fuel cask using fewer detector locations is therefore desirable. This work presents the development of a self-occluding neutron detector system that can reliably monitor the direction of movement of a spent fuel cask from few locations. The IAEA continuously aims to improve efficiency and effectiveness when implementing Safeguards under its mandate. Therefore, UMS design considerations include cost, reliability, and the ease of interpretation of measurement results for efficiently supporting the drawing of safeguards conclusions.

Introduction

Despite the advancement of geological disposal projects, such as those in Finland and Sweden, the amount of spent nuclear fuel under international safeguards in dry storage continues to accumulate [1]. Once spent fuel is loaded into a dry cask and the cask is closed, it becomes difficult to access the nuclear material inside for reverification. Therefore, a significant effort is made to maintain continuity of knowledge on dry casks for safeguards purposes [2]. Continuity of knowledge is achieved through surveillance, containment, and monitoring. In particular, unattended monitoring systems (UMS) are used in monitoring dry cask movements between and within facilities. UMS provide advantages by reducing inspection efforts, reducing radiation exposure to inspectors, and reducing the level of intrusiveness to the operation of nuclear facilities [3].

Monitoring the movement of casks within a facility using UMS can be achieved by placing multiple neutron detectors and observing the count rate changes as the cask moves past the detectors. However, in certain cases, there are limited options for positioning the detectors. Additionally, installing and maintaining multiple detector emplacements adds complexity and cost. Therefore, there is an advantage in tracking the movement of casks using fewer detector locations. This paper reports simulation results that demonstrate the ability to discriminate between cask movement paths from a single detector location using a self-occluding detector based on standard He-3 proportional counters and high-density polyethylene (HDPE).

Methods

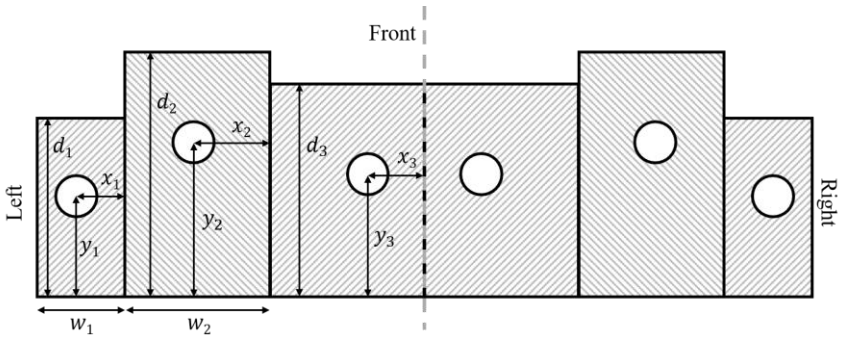

Figure 1. Diagram illustrating the horizontal cross section of a hypothetical candidate detector design. The circles indicate the position of the 6 He-3 tubes. The 11 optimization parameters are shown: 2 HDPE block widths (w_1 and w_2), 3 HDPE block depths (d_1, d_2, and d_3), 3 He-3 tube x-coordinates (x_1, x_2, and x_3), and 3 He-3 tube y-coordinates (y_1, y_2, and y_3). The center dashed line indicates the plane of symmetry.

A common design used for IAEA neutron monitors is a slab of HDPE containing one or more rows of He-3 tubes. Because the neutron flux generally decreases with distance from a cask, the He-3 tubes within a slab that are closest to a cask generate the highest count rate. Therefore, by comparing the count rates of the tubes at opposite ends of the rows of He-3 tubes, a relative determination of cask position could be achieved. However, the usual slab design is not well suited to take advantage of this effect. Additionally, while the HDPE acts as a neutron moderator in a standard slab design, in larger thicknesses, it can also act as a neutron shield. By changing the shape of the HDPE and repositioning the He-3 tubes, the HDPE can be used to occlude the view of He-3 tubes on one side of the detector to neutron sources on the opposite side of the detector. This would enhance the ability of the detector to discern the position of a cask.

To modify a standard slab design for this purpose, several constraints were imposed. First, the design was limited to 6 He-3 tubes for cost considerations. The tubes were grouped into three pairs consisting of one left group, one center group, and one right group. The output signals from each pair of He-3 tubes are daisy chained together to provide one input to a data acquisition module per group. While two groups would be sufficient to discriminate between left-to-right and right-to-left motion, the design is required to still discriminate direction of motion in the case that any one group fails; so, three groups are used. Left-right symmetry was imposed on the design. For simplicity of design and fabrication, each He-3 tube is embedded within a block of HDPE with equal heights and aligned backs. The depth and width of each block of HDPE were considered as parameters for optimization, as were the coordinates of the center of the He-3 tube within each block of HDPE. The depth of each HDPE block was limited to a maximum of 17 cm and the total width of the HDPE blocks was fixed to 54.8 cm. Therefore, there are 11 parameters for optimization: 2 for the widths of HDPE blocks, 3 for the depths of HDPE blocks, 3 for He-3 x-coordinates, and 3 for He-3 y-coordinates. The optimization parameters are illustrated in Figure 1. Additionally, cadmium sheets were added around the sides of the detector to reduce the detector's sensitivity to background and neutrons scattered in the environment.

To optimize the parameter values, a Python script was written to generate simple MCNP6 [4] input decks for a given parameter set and cask position. For each parameter set, a series of 12 cask positions are simulated along a 400 cm line 200 cm from the detector face, as shown in Figure 2. Because of the left-right symmetry of the detector, these simulated positions effectively cover 23 positions along an 800 cm path in which a cask passes the detector at a distance of 200 cm. The

cask is modeled as a neutron emitter from a cylindrical surface that is 250 cm in diameter and 580 cm tall. The direction of each emitted neutron is selected by sampling its direction cosine, relative to the surface normal, from a flat distribution. The emitted neutron energy spectrum was generated by simulating the attenuation of Watt spectrum neutrons through the geometry of a proprietary cask design and tallying the energy spectrum of neutrons exiting the cask's surface. The resulting spectrum is similar to measured spectra reported in literature [5].

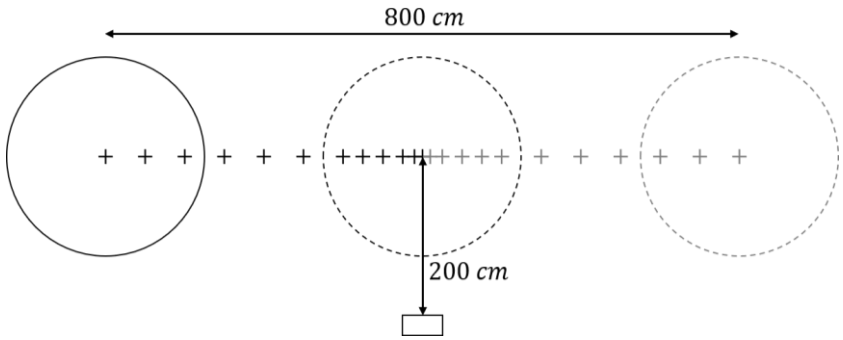

Figure 2. Diagram illustrating the 12 simulated cask positions for each detector design iteration, shown in black. The cask positions were centered 200 cm perpendicularly from the face of the detector and each offset laterally from the center by 0 cm, 10 cm, 25 cm, 50 cm, 75 cm, 100 cm, 150 cm, 200 cm, 250 cm, 300 cm, 350 cm, and 400 cm. The gray positions indicate those implicitly simulated by symmetry. The circles illustrate the 250 cm cask diameters, shown at the beginning, center, and end of the path, for clarity.

For each MCNP simulation, the neutron count rate for each tube is approximated as,

$$\dot{C}_t = \dot{n}TV, \tag{1}$$

where $\dot{C}_t$ is the count rate in tube t, $\dot{n}$ is a nominal cask side neutron emission rate of 10^8 neutrons per second, T is the F4 cell flux tally for the active volume of tube t with an (n, p) reaction multiplier, and V is the tube's active volume. The resulting design is not sensitive to the choice of $\dot{n}$; it only serves to provide a more physical interpretation of the intermediate results. The pairs of tubes in each group are summed together to produce count rates for the left, center, and right groups.

To account for cask movement during measurement and discrete measurement intervals, a constant cask speed of 50 cm/s is assumed and 1 s measurement times are used. The cask speed is used to convert from group count rates vs position to group count rates vs time, which is then integrated over consecutive 1 s intervals, using linear interpolation between simulated points, to get simulated group total counts. Group total count data points most closely represent the data that would actually be available for analysis from a physical measurement. The simulated total counts during a cask passage for the optimal design iteration are plotted in Figure 3.

A figure of merit (FOM) for each detector design is based on the certainty in the difference between the ratio (R_i) of the left and center groups' total counts ($C_{L,i}$ and $C_{C,i}$) at two points, i, during the cask passage. The ratio, R_i, is calculated as,

$$R_i = C_{L,i}/C_{C,i}, \tag{2}$$

with an associated variance, $\sigma_{R_i}^2$,

$$\sigma_{R_i}^2 = R_i^2\left(\frac{1}{C_{L,i}} + \frac{1}{C_{C,i}}\right). \tag{3}$$

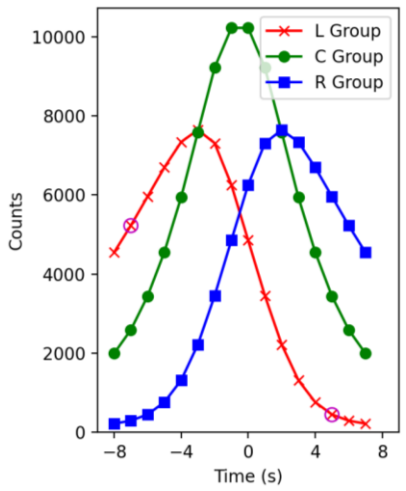

Figure 3. Simulated counts vs time for each of the three He-3 tube groups for the detector design with the largest FOM. The data points for the left group at which z is at its maximum and minimum are circled.

For each data point along the path, the number of standard deviations R_i is from unity, z_i, is calculated,

$$z_i = \frac{R_i - 1}{\sigma_{R_i}}. \quad (4)$$

The simulated R, σ_R, and z values during a cask passage for the optimal design iteration are plotted in Figure 4. When z_i is positive, a larger value indicates a higher level of certainty in a measurement that $C_{L,i}$ is greater than $C_{C,i}$. When z_i is negative, a more negative value indicates a higher level of certainty that $C_{L,i}$ is less than $C_{C,i}$. The point where z_i is smallest is assigned $i = S$ and the point where it is largest is assigned $i = L$. These data points are used to calculate the FOM,

$$FOM = \frac{R_L - R_S}{\sqrt{\sigma_{R_L}^2 + \sigma_{R_S}^2}}. \quad (5)$$

The design with the largest FOM has the greatest certainty in the difference of the ratios at two points along the cask's path. For each design iteration, the FOM is calculated. Then, of all the designs that have been simulated, the one with the largest FOM is used as the basis for the next design iteration. The next iteration is generated with a randomly assigned perturbation of one or more of the 11 optimization parameters of the design with the largest FOM. Optimization parameter value sets are not repeated.

Results

Trials of the optimization process were iterated within the time constraints of the project and the resulting design with the largest FOM is depicted in Figure 5. The corresponding

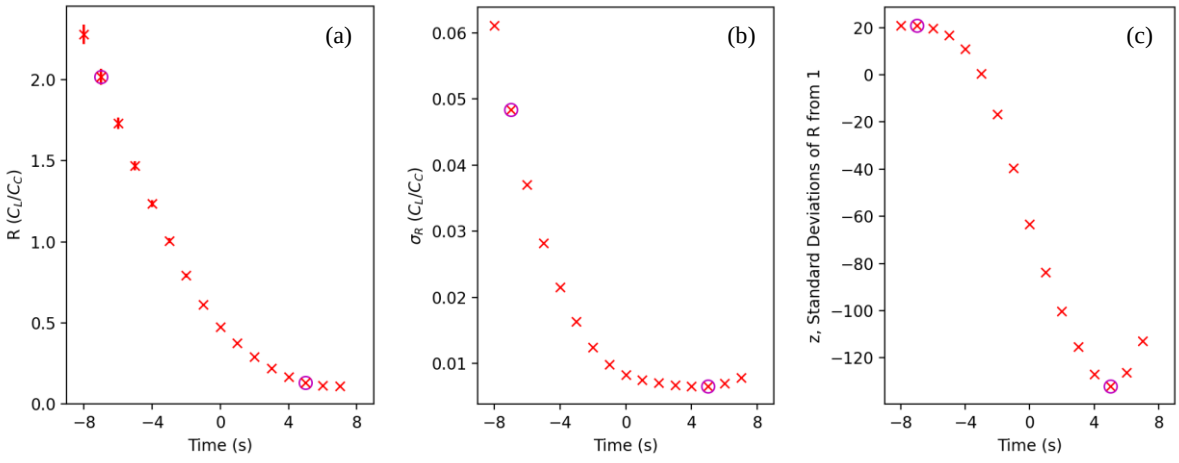

Figure 4. (a) R vs time, (b) σ_R vs time, and (c) z, the number of standard deviations R is from 1, vs time for the optimal design iteration. The data points at which z is at its maximum and minimum are circled.

optimization parameter values are listed in Table 1. The simulated total counts for the design during a cask passage are plotted in Figure 3 and the corresponding R, σ_R, and z values are plotted in Figure 4. Initially, the cask is to the left of the detector, so C_L is larger than C_C (and C_R) and R is therefore greater than 1. As the cask gets closer to the detector, the relative increase in C_C is larger than the relative increase in C_L so R decreases. However, because the counts are increasing for both groups, the relative uncertainty in R decreases, initially causing an increase in z. As the cask continues approaching the detector, eventually C_C catches up with C_L, resulting in an R of 1 and thus a z of 0. As the cask passes the center of the detector, C_C reaches its maximum value while C_L is decreasing, making R continue to decrease and z to become negative. As the cask continues to the right of the detector, C_c decreases but initially at a slower rate than C_L. This results in a decrease of R so z continues decreasing until the relative uncertainty in C_C and C_L becomes significant because of the small number of counts. Eventually, z reaches a minimum and begins to increase as R becomes less statistically distinguishable from 1. The data points where z is at a minimum or maximum are circled in the plots in Figures 3 and 4. The FOM, calculated using these points and Eq. 5, is 38.6.

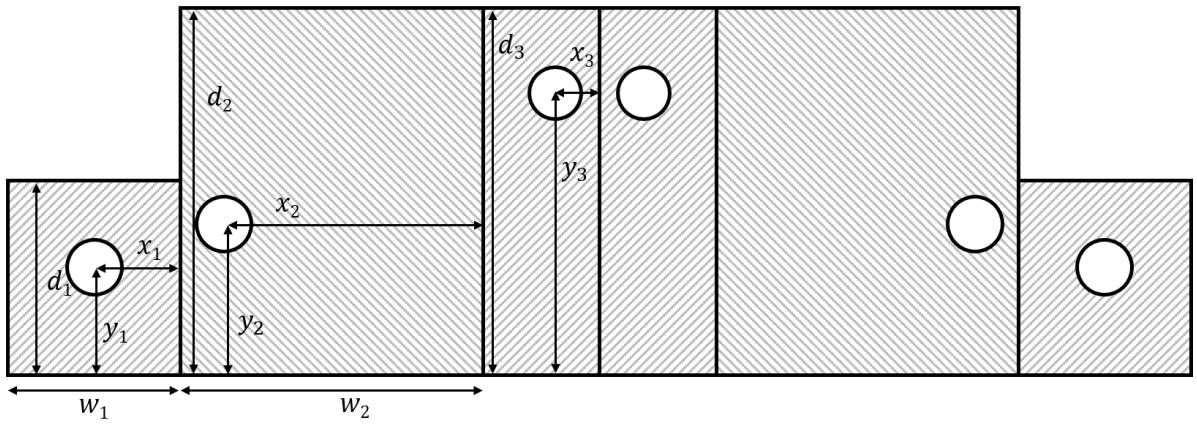

Figure 5. Diagram illustrating the horizontal cross section of the end detector design. The circles indicate the positions of the 6 He-3 tubes. The 11 optimization parameters are shown: 2 HDPE block widths (w_1 and w_2), 3 HDPE block depths (d_1, d_2, and d_3), 3 He-3 tube x-coordinates (x_1, x_2, and x_3), and 3 He-3 tube y-coordinates (y_1, y_2, and y_3).

Table 1. Final Values of the Optimization Parameters in cm

w_1	w_2	d_1	d_2	d_3	x_1	x_2	x_3	y_1	y_2	y_3
8	14	9	17	17	5	7	13	4	12	2

Further simulations with additional detail were performed to estimate the performance of the detector design in a more realistic scenario. In this scenario, the detector is positioned, facing north, near a doorway in a concrete wall, to the east, that separates rooms within a facility. The purpose of the detector in this scenario is to determine whether a cask passes through the doorway and, if so, in which direction. A simplified diagram of the geometry in the scenario and two simulated cask paths are shown in Figure 6. The first path is a west-to-east path in which the cask

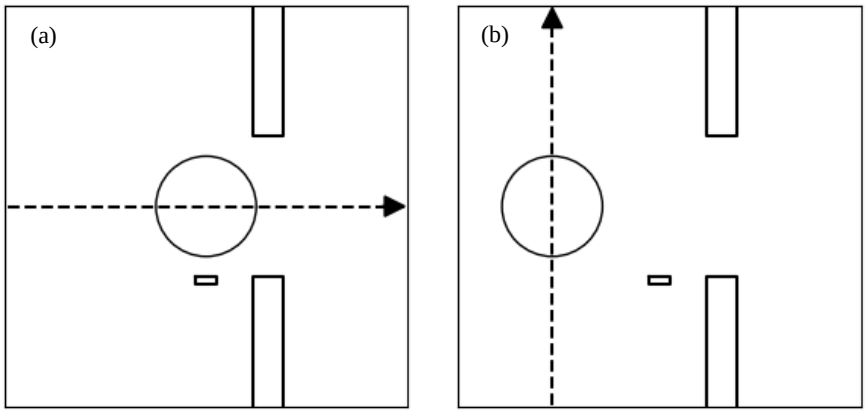

Figure 6. Diagrams of the (a) west-to-east and (b) south-to-north simulated cask paths. The walls around the doorway on the east (right) side and the detector to the west side of the walls are shown in both diagrams. The outer perimeter of a cask on each path is also shown.

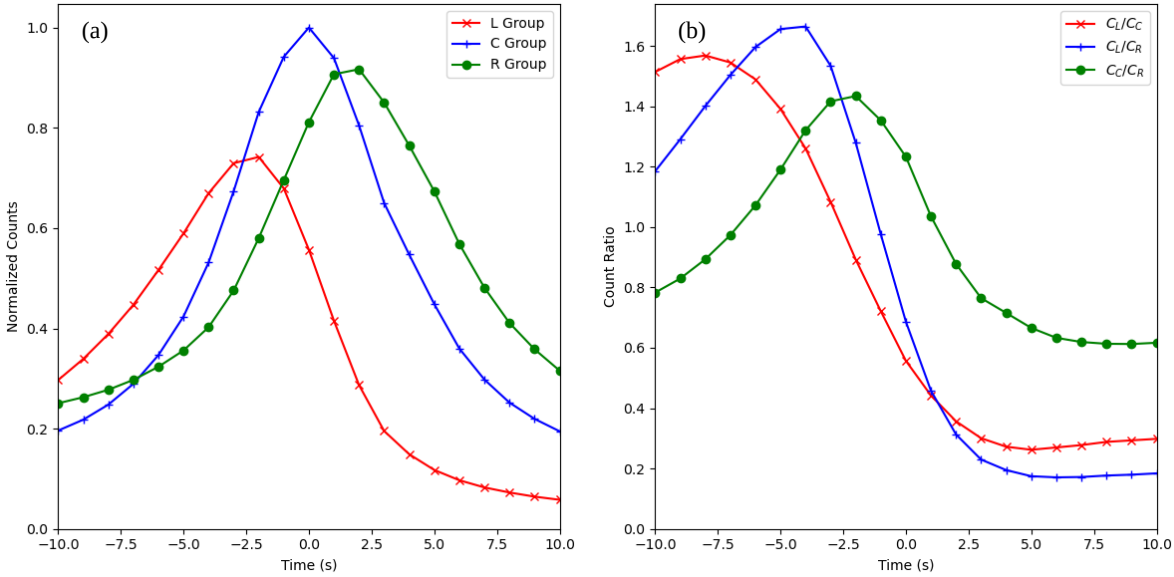

Figure 7. Plots of (a) normalized counts vs time and (b) count ratios vs time for the simulated west-to-east path. 0 s corresponds to the time at which the cask is centered on the detector's face (as shown in Figure 6.a.). Counts are normalized to the center group's maximum value.

passes by the face of the detector and continues through the doorway. The second path is a south-to-north path in which the cask passes by the left side of the detector without entering the doorway.

Simulated results for the west-to-east path are plotted in Figure 7. The features of this path seen in Figure 7(a) are similar to those in Figure 3, as described above. In this case, however, there is some asymmetry, with the counts in the right group being disproportionately increased by the nearby wall which reflects neutrons from the cask back toward the detector. Nonetheless, the same basic trends in the data are seen as the cask passes the detector. The plots of the three ratios shown in Figure 7(b) illustrate a key design point of the detector design: any one of the three groups can fail and a ratio of counts from two groups can still be constructed which decreases from above

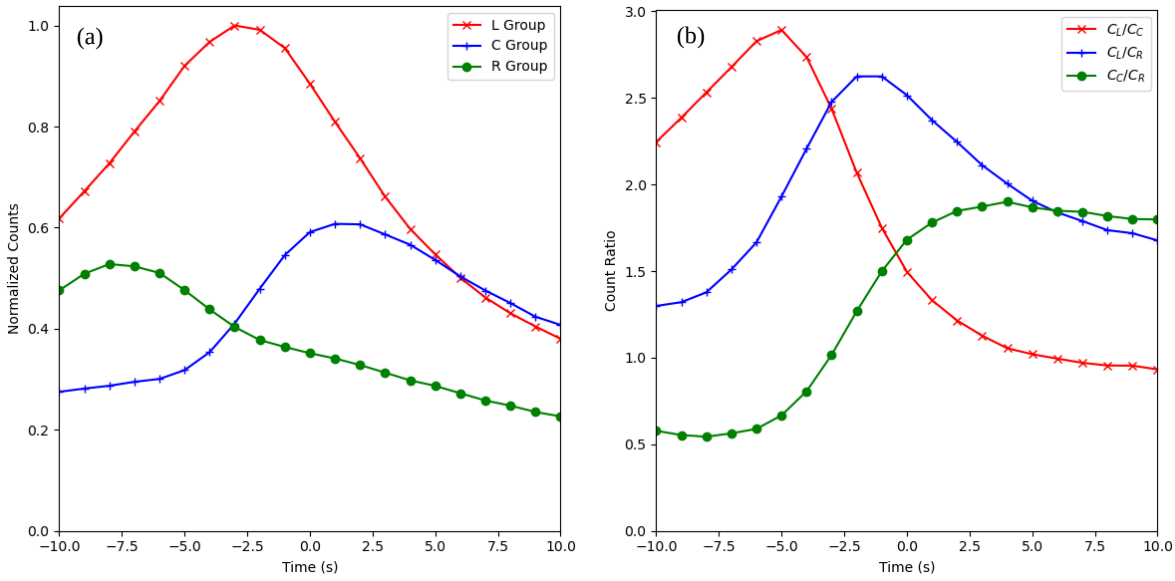

Figure 8. Plots of (a) normalized counts vs time and (b) count ratios vs time for the simulated south-to-north path. 0 s corresponds to the time at which the cask crosses the west-to-east path (as shown in Figure 6.b.). Counts are normalized to the center group's maximum value.

1.25 to below 0.75 as the cask moves from left to right past the detector. Conversely, those same ratios would increase from below 0.75 to above 1.25 if the cask were to move past the detector in the opposite direction. So, a west-to-east cask movement would be easily distinguishable from an east-to-west cask movement.

Simulated counts for the south-to-north path are shown in Figure 8(a). As the cask approaches the left side of the detector, the counts in the left group increase. However, the counts in the right group decrease because of the increased attenuation from the bulk of HDPE between it and the cask. The center group counts initially increase only slowly but as the cask passes the side of the detector, they increase sharply. After the cask passes the side of the detector and continues moving away from it, the counts from all three groups decrease. The count ratios for this path are shown in Figure 8(b). For both ratios that make use of the left group, the ratios do not decrease below 1.25, clearly distinguishing the patterns from those shown in Figure 7.b. in which the cask travels past the face of the detector. While the C_C/C_R alone could be mistaken for the reverse of the path shown in Figure 7.b., the counts from the right group reach a maximum while C_C/C_R is near its minimum, which is the opposite of the pattern seen when a cask travels past the face of the detector. So, the south-to-north path is easily distinguishable from the west-to-east path or east-to-west path using signals from any two of the three detector groups in the detector.

Conclusions

A self-occluding directional neutron detector based He-3 proportional counters has been designed. Simulations have demonstrated its potential suitability for dry cask monitoring for international safeguards purposes. The design has built-in redundancy that eliminates a single point of failure and is based on proven reliable components, making it immediately suitable for unattended measurements. The analysis of data collected by the detector can be automated to allow

for efficient safeguards. Based on these results, a prototype is being constructed and testing will be performed.

For an accurate assessment of the performance of the detector in a particular facility, an uncertainty analysis needs to be performed. This analysis would need to consider the background and source strengths expected at the particular facility.

It is a significant challenge to optimize a complicated function of 11 parameters where each parameter set evaluation is computationally expensive. While the design resulting from this work performs much better than any of the designs initially considered, it is not asserted to be the absolute optimal design. Furthermore, the choice of constraints in which the He-3 detectors are placed in rectangular HDPE blocks likely limits the potential performance as compared to an optimized design with fewer geometry restrictions. So, further optimization of the detector design could be done by improving the efficiency of the optimization process and loosening the geometry constraints.

References

[1] IAEA, "Status and Trends in Spent Fuel and Radioactive Waste Management, Nuclear Energy Series No. NF-T-3.1," IAEA, Vienna, 2018.

[2] IAEA, "International Safeguards in the Design of Facilities for Long Term Spent Fuel Management, Nuclear Energy Series No. NW-T-1.14," IAEA, Vienna, 2018.

[3] R. Abedin-Zadeh and J. Whichello, "Remote and unattended monitoring techniques," in *Technical workshop on safeguards, verification technologies, and other related experience*, Vienna, 1998.

[4] C. J. Werner, "MCNP6.2 Release Notes, Los Alamos National Laboratory report," LA-UR-18-20808, 2018.

[5] A. Rimpler, "Bonner sphere neutron spectrometry at spent fuel casks," *Nuclear Instruments and Methods in Physics Research,* vol. 476, pp. 468-473, 2002.